Attosecond Resolved Electron Release in Two-Color Near-Threshold Photoionization of N_2

Jérémie Caillat,[1,2] Alfred Maquet,[1,2] Stefan Haessler,[3,4] Baptiste Fabre,[5] Thierry Ruchon,[3] Pascal Salières,[3] Yann Mairesse,[5] and Richard Taïeb[1,2]

[1]*UPMC Université Paris 6, UMR 7614, Laboratoire de Chimie Physique-Matière et Rayonnement, 11 rue Pierre et Marie Curie, 75231 Paris Cedex 05, France*

[2]*CNRS, UMR 7614, LCPMR, Paris, France*

[3]*CEA-Saclay, IRAMIS, Service des Photons, Atomes et Molécules, 91191 Gif-sur-Yvette, France*

[4]*Photonics Institute, Vienna University of Technology, Gusshausstrasse 27, A-1040 Vienna, Austria*

[5]*CELIA, UMR 5107 CNRS, Université Bordeaux I, CEA, 351 Cours de la Libération, 33405 Talence, France*

(Received 28 September 2010; published 1 March 2011)

We have simulated two-color photoionization of N_2 by solving the time-dependent Schrödinger equation with a simple model accounting for the correlated vibronic dynamics of the molecule and of the ion N_2^+. Our results, in very good agreement with recent experiments [Haessler *et al.*, Phys. Rev. A **80**, 011404 (2009)], show how a resonance embedded in the molecular continuum dramatically affects the phases of the two-photon transition amplitudes. In addition, we introduce a formal relation between these measurable phases and the photoelectron release time, opening the way to attosecond time-resolved measurements, equivalent to double-slit experiments in the time domain.

DOI: 10.1103/PhysRevLett.106.093002 PACS numbers: 33.20.Xx, 33.80.Rv

Measurements and analysis of the cross sections for inelastic processes in the vicinity of a resonant frequency are invaluable tools to explore the structure and dynamics of reactive states in microscopic systems. An imposing corpus of references devoted to the analysis of resonance spectra [1] starting from the decay of unstable nuclei [2], covers Feshbach resonances observed in ultracold gases [3] and atomic and molecular phenomena involving autoionizing states [4]. The widths of the lines in the dispersion curves obtained in the energy domain give access to the lifetimes of the probed excited states. In the last ten years, the advent of harmonic sources delivering uv and extreme ultraviolet (xuv) pulses with attosecond durations (1 as $= 10^{-18}$ s) opened the way to real-time tracking of such ultrafast electronic processes, as first demonstrated in the case of Auger lifetimes in atoms [5] and more recently in the case of photoionization processes in solids [6] or molecules [7].

Such measurements in the attosecond time domain have been achieved via two-color infrared–extreme ultraviolet (ir-xuv) photoionization experiments. Based on the combination of isolated attosecond xuv pulses with few-cycles ir pulses, the so-called streaking technique [5,8,9] provides a time resolution of a few attoseconds on the ionization timing. Using longer pulses, the so-called RABBIT technique [10] gives access to phase differences that are intrinsically linked to time delays. It has been successfully used to characterize attosecond pulse trains [10–12] or to recover information on the ionized system itself [13–15]. In the latter case, the adequate interpretation of the time delays so derived remains unclear.

In this Letter, we focus on the RABBIT technique, addressing two major issues: how a resonance may affect the phase of the two-photon ionization amplitude, and what is the temporal information encoded in that phase. The RABBIT method is based on the ''multicolor'' ionization of a gas in the presence of a low intensity ir field, with a comb of its odd xuv harmonics. In these conditions, the photoelectron spectrum displays equidistant peaks coming from the absorption of one harmonic photon, labeled $(\ldots, H_{2q-1}, H_{2q+1}, \ldots)$, and intermediate sidebands $(\ldots SB_{2q} \ldots)$ resulting from xuv-ir two-photon transitions. Two quantum paths contribute dominantly to the formation of a given sideband SB_{2q}: (i) sequential absorption of H_{2q-1} and of the fundamental and (ii) absorption of H_{2q+1} followed by stimulated emission of the fundamental [16]. The RABBIT method consists in monitoring the sideband intensity oscillations resulting from the two paths' interferences, when the ir-xuv delay τ is varied. In its conventional implementations, a reference atom, with a smooth continuum, is used as a target: measuring the phases of the oscillations gives access to the relative phases of the harmonics and, by extension, to their emission time, with attosecond resolution [10,12].

With objective to probe in the time domain the photoelectron emission from a molecule, the method was recently implemented in an unusual manner [14]: an ir pulse and its odd harmonics with known phases were used to ionize N_2, which possesses a rich and structured continuum. Depending on the vibronic photoionization channel, the measured RABBIT phases presented a nontrivial behavior. This was attributed to the presence of a resonance embedded in the continuum, yet the relation between the RABBIT phases and the timing of the electron emission remained to be established.

Here, we present the results of simulations performed with a model system accounting for the relevant vibronic

 © 2011 American Physical Society

dynamics of N_2 and N_2^+. In very good agreement with the experimental data [14], these results not only supply a clear understanding on how the resonance affects the vibrationally resolved phases, but also they demonstrate how RABBIT measurements can reveal the attosecond resolved timing of a complex photoionization process. Moreover, the presence of the resonance produces a nice example of a double-slit interference in the time domain, associated with quantum path interferences.

The two-dimensional (2D) model reproduces the essential features of N_2 and N_2^+, namely, the vibronic energies of the ground state (hereafter referred to as G) and of the resonant state of interest (R) in N_2, and of the $X\,^2\Sigma_g^+$ (X) and $A\,^2\Pi_u$ (A) states in N_2^+. The R state is an autoionizing state belonging to the Rydberg series converging to the $B\,^2\Sigma_u^+(3d\sigma_g)\,^1\Sigma_u^+$ Hopfield state of the ion [17], which mostly couples to the X ionization channel. In the following, each of the considered vibronic state is designated by its corresponding electronic and vibrational labels, i.e., $|G, v\rangle$, $|R, v''\rangle$, $|X, v'\rangle$, and $|A, v'\rangle$. Our model, similar to the one used in [18], consists in an active electron with coordinate x and an ionic core with internuclear separation ρ and reduced mass $\mu = 7$ amu. For a given electronic channel, the Hamiltonian reads, in atomic units (a.u.),

$$H_0 = -\frac{1}{2\mu}\frac{\partial^2}{\partial\rho^2} + V_c(\rho) - \frac{1}{2}\frac{\partial^2}{\partial x^2} + V_e(x, \rho). \quad (1)$$

The ionic core potential $V_c(\rho)$ is associated with the Born-Oppenheimer (BO) energy of the ion in the considered channel. The electron-core potentials $V_e(x, \rho)$ were adjusted to reproduce the ρ-dependent BO energies [19] of the neutral, i.e., the G electronic energy when considering the A channel, and the G and R energies when considering the X channel. Within this single-active electron model, the autoionizing state is represented by a shape resonance with proper energy and width [20], obtained by adjusting a ρ-dependent barrier above threshold in the electron-core potential of the X channel [see Fig. 1(a) for a cut of V_e at $\rho = 2$ a.u.]. The resonance width $\Gamma_R \approx 11$ meV, corresponding to a lifetime of $\sim$60 fs, was adjusted on the data of [17]. We have neglected couplings between channels, which are very unlikely to occur in the relatively low intensity regime of a RABBIT measurement. Figure 1(b) displays the BO curves obtained with the optimized potentials for both channels, as well as a few vibrational levels. Vibrational separations are roughly 290, 270, and 230 meV in the R, X, A electronic states, respectively.

For each electronic channel, the time evolution of the model molecule interacting with the light fields is given by the time-dependent Schrödinger equation:

$$i\frac{\partial\Psi(x, \rho, t)}{\partial t} = [H_0 + W_\tau(t)]\Psi(x, \rho, t), \quad (2)$$

where $\Psi(x, \rho, t)$ is the time-dependent vibronic wave function and $W_\tau(t)$ is the dipole coupling with the light pulses. The latter is characterized by the time delay τ between the maxima of the xuv and ir envelopes. We used $\cos^2$ envelopes with FWHM durations of approximately 25 and 40 fs for the xuv and ir pulses, respectively, both with intensities within the linear regime.

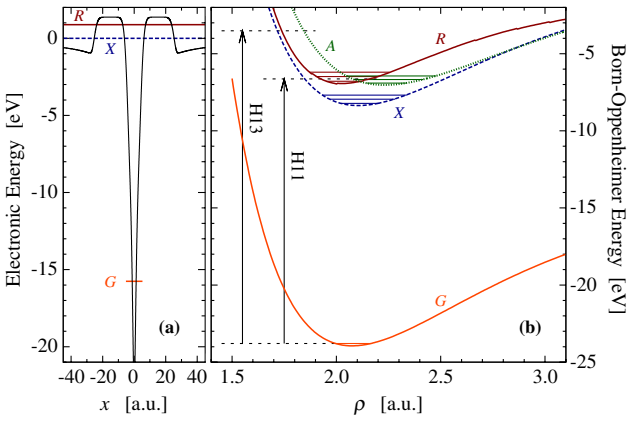

FIG. 1 (color online). (a) Electron-nuclei potential $V_e(x, \rho)$ for the X channel, cut at $\rho = 2$ a.u. (black full curve). Horizontal lines indicate the ground (G) and resonant (R) electronic energies as well as the ionization threshold (X). (b) Relevant molecular energies of the model treated in the BO approximation, for the X and A ionization channels. Horizontal lines indicate the first few vibrational energies of each curve. Vertical arrows indicate the photon energies corresponding to harmonics 11 and 13 of $\omega_L = 1.56$ eV.

We solved Eq. (2) by expanding $\Psi(x, \rho, t)$ as

$$\Psi(x, \rho, t) = \sum_{v'=0}^{N-1} f_{v'}(x, t)\chi_{v'}(\rho). \quad (3)$$

Here, the functions $\chi_{v'}(\rho)$ are associated with the N first vibrational states of the ionic core, i.e., eigenfunctions of the first two terms of H_0 in Eq. (1), while $f_{v'}(x, t)$ are v'-dependent electronic wave packets. This representation of $\Psi(x, \rho, t)$ provides a compact way of dealing with its ρ dependence, as only a few vibrational states of the ion are populated (typically $N < 10$), and gives access directly to v'-resolved observables for each electronic channel. Ionization probabilities and electron spectra were extracted from $f_{v'}(x, t)$ propagated after the end of the radiation pulses until the influence of the ionic core on the ejected electron becomes negligible. The RABBIT phases θ_{2q} were deduced by fitting the evolution of the sideband SB_{2q} in the electron spectra against the delay τ with the generic function

$$g_{2q}(\tau) = a + b\cos(2\omega_L\tau + \theta_{2q}), \quad (4)$$

where ω_L is the fundamental ir frequency [21].

The channel-dependent RABBIT phases obtained with $\omega_L = 1.56$ eV, close to the frequency used in [14], are displayed in Fig. 2 and compared with the experimental ones. For all the considered sidebands (SB_{12-18}), the phases in the A channel remain above -0.3π rad and go monotonically to zero with increasing harmonic order, with practically no dependence on the final vibrational state v'. These variations are representative of the ones

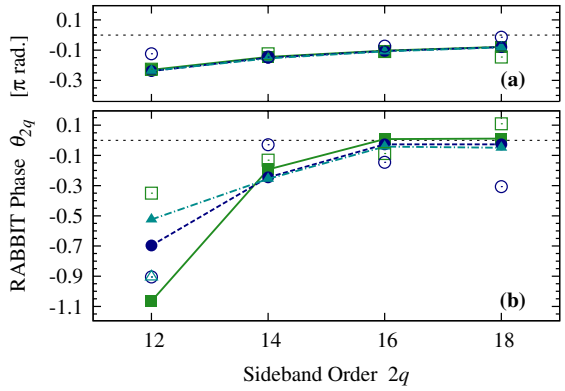

FIG. 2 (color online). v'-resolved RABBIT phases associated with the sidebands 12 to 18 at $\omega_L = 1.56$ eV: (a) A channel, (b) X channel. Values corresponding to $v' = 0$, 1, and 2 are indicated by squares, circles, and triangles, respectively. Full symbols connected with straight lines correspond to theoretical results, while empty symbols correspond to the experimental data taken from [14].

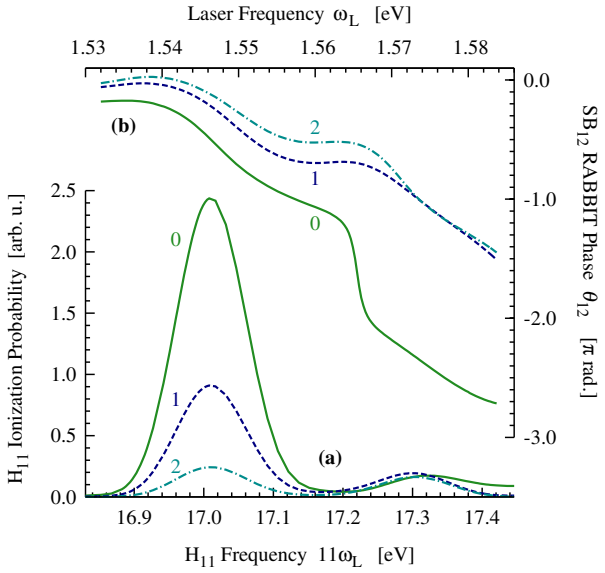

FIG. 3 (color online). (a) v'-resolved probability to photoionize the model molecule in the X channel with the 11th harmonic against the laser frequency, in the vicinity of the resonance. (b) X channel v'-resolved SB_{12} RABBIT phases in the same range of frequencies. In both frames, each curve is labeled by the corresponding final vibrational state v'.

obtained with a smooth continuum. The same is observed in the X channel for all sidebands but SB_{12}. Indeed, the latter presents important and unusual shifts, down to $-\pi$ rad, which strongly depend on v'. For that value of ω_L, H_{11} is expected to hit the continuum between the first two vibrational states of the resonance [see Fig. 1(b)], thus affecting the subsequent transition towards SB_{12}. The agreement between simulations and experiments is excellent in the A channel. It remains very satisfactory in the X channel, although the SB_{12} phase dependency on v' is different—which can be ascribed to the extreme sensitivity of the phase on the precise value of the laser frequency when scanning a resonance, as seen below.

To clarify the effect of the resonance on the RABBIT phase changes, we varied ω_L between 1.53 and 1.58 eV in our simulations, allowing H_{11} to finely scan the vicinity of the resonance, now focusing exclusively on the X channel. Figure 3(a) displays the v'-resolved ionization probability with H_{11} alone, as a function of ω_L. For each v', the curve exhibits two peaks approximately located at $11\omega_L = 17.0$ and 17.3 eV, corresponding to ionization through the resonant states $|R, v'' = 0\rangle$ and $|R, v'' = 1\rangle$, respectively. Note that the H_{11} bandwidth, of about $\sim$0.15 eV, is 1 order of magnitude larger than Γ_R and governs the width of the photoelectron peaks. We verified that the ionization probability at each peak is proportional to the corresponding Frank-Condon (FC) product $|\langle X, v'|R, v''\rangle\langle R, v''|G, 0\rangle|^2$. Because of much smaller FC overlap with the ground state, the resonant states $v'' > 1$ do not contribute. These results indicate that, when ω_L varies, H_{11} probes two neighboring resonances, $|R, 0\rangle$ and $|R, 1\rangle$, respectively, with relative ionization efficiencies depending on the final state $|X, v'\rangle$ of the ion.

The SB_{12} phases in the same frequency range are shown in Fig. 3(b). Their evolution are linked to the H_{11} ionization probabilities: each v'-resolved phase displays a smooth $\sim -\pi$ jump as H_{11} crosses the resonances, around $\omega_L = 1.546$ and 1.574 eV, respectively. Between them, the phase evolution depends strongly on v': it remains almost flat for $v' = 1$ and 2, while it goes through a stiff $-\pi$ jump at $\omega_L = 1.565$ eV for $v' = 0$ [22].

As explained in [14], the second-order perturbative treatment of two-photon ionization predicts that, when varying the frequency, a π jump occurs in the RABBIT phase θ_{2q} when one of the adjacent harmonic crosses a resonance. An additional π jump is expected between two resonances, at the frequency where their respective contributions compensate each other. Therefore, when changing the frequency and scanning two resonances, three phase jumps are expected: two are located at the resonant energies, the third one being in between. This latter jump may be seen or not, depending on the resonance parameters, namely, on their widths and magnitudes, and also on the intrinsic resolution of the pump pulse. This is well illustrated in our simulations, where the relative magnitudes of the two neighboring resonances vary significantly with v': The ionization peak ratio, governed by the corresponding FC factors, is 15:1 for $v' = 0$ while it is 5:1 and 2:1 for $v' = 1$ and 2, respectively. This leads to the appearance of the intermediate phase jump for $v' = 0$ while it is absent for $v' = 1$ and 2.

To uncover the relation between the sideband phase behavior and the electron release timing, we have performed additional two-color simulations where the xuv pulse consists of a single harmonic, either H_{11} or H_{13}. Then, we estimated the SB_{12} formation times through the H_{11} and H_{13} paths, respectively τ_{11} and τ_{13}. This was achieved in our simulations by determining the arrival

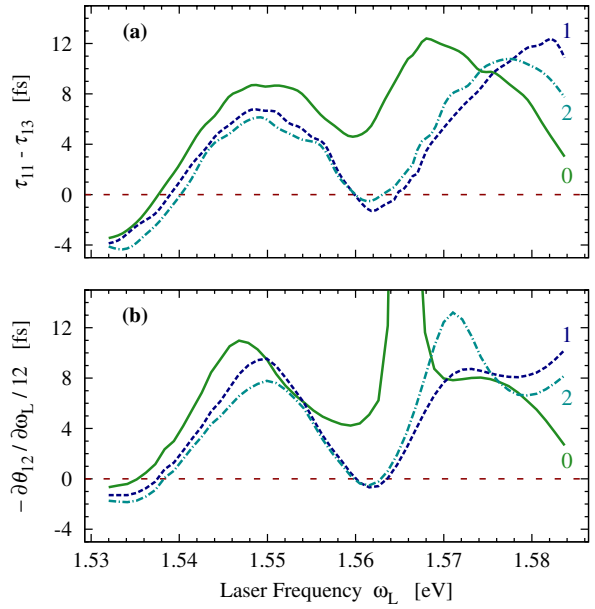

FIG. 4 (color online). (a) v'-resolved SB_{12} formation delay in the X channel versus ω_L. (b) v'-resolved SB_{12} RABBIT phases derivative with respect to the corresponding ω_L-dependent photoelectron energy [see Eq. (5)]. Labels indicate the final vibrational state v' as in Fig. 3.

times of the corresponding electronic wave packets, at a distance where they no longer experience the influence of the core. The time difference between the two paths, $\Delta\tau_{12} = \tau_{11} - \tau_{13}$, is displayed for each final vibrational state v' in Fig. 4(a). The formation time turns out to be strongly affected by the resonances: when H_{11} hits either $|R, 0\rangle$ or $|R, 1\rangle$, we find that the SB_{12} formation is delayed by several femtoseconds as compared to the nonresonant path involving H_{13}. Moreover, the variations of $\Delta\tau_{12}$ between the resonances clearly depends on v': it remains large and positive for $v' = 0$, while it takes negative values around $\omega_L = 1.56$ eV for $v' = 1$ and 2.

A "time-of-flight" simulation with such an ultrashort time resolution corresponds to a gedanken experiment: its realization is well beyond the capabilities of current detection methods. It can, however, be shown that $\Delta\tau_{2q}$ is related to the change of the RABBIT phase when varying the energy of the driving laser frequency (i.e., of the photoelectron kinetic energy E_{2q}) [23]:

$$\Delta\tau_{2q} = -\hbar\frac{\partial\theta_{2q}}{\partial E_{2q}} = -\frac{\partial\theta_{2q}}{2q\partial\omega_L}. \quad (5)$$

We have thus taken the derivative of the phases displayed in Fig. 3(b). The resulting times, shown in Fig. 4(b), are in excellent agreement with the ones shown in Fig. 4(a), with comparable v' dependencies. The same delays of ~8 fs are obtained around the resonant frequencies ($\omega_L \simeq 1.546$ and 1.574 eV), and the same crossings of the 0 delay line are obtained before the resonances ($\omega_L \lesssim 1.538$ eV) for all v', and between the resonances ($\omega_L \simeq 1.562$ eV) for $v' = 1$ and 2. Moreover, the steep π jump observed between the resonances only for $v' = 0$ induces a delay exceeding 12 fs. The phase derivative at this frequency is much larger than the "measured" time, the latter being bounded by the durations of the ir and xuv pulses.

In summary, relying on a simple model designed to represent the vibronic dynamics of N_2, we have investigated how a near-threshold resonance affects vibrationally resolved two-color photoionization phases in a molecular RABBIT measurement. We have found that the photoemission dynamics is strongly modified by the presence of an intermediate resonance and shown how experimentally observable data, i.e., the RABBIT phases, can be exploited to retrieve the attosecond photoelectron release profile. We would like to emphasize that such time-resolved measurements are nowadays feasible, thanks to the development of tunable intense ir sources combined with accurate detection methods [15].

We acknowledge financial support from the ANR-09-BLAN-0031-01 ATTO-WAVE program. Parts of the computations have been performed at IDRIS. This research was supported in part by the National Science Foundation under Grant No. NSF PHY05-51164.

[1] N. Mott and H. Massey, *The Calculation of Atomic Collision Processes* (Oxford University Press, Oxford, 1965).
[2] H. Feshbach, Ann. Phys. (N.Y.) **5**, 357 (1958).
[3] C. Chin *et al.*, Rev. Mod. Phys. **82**, 1225 (2010).
[4] U. Fano, Phys. Rev. **124**, 1866 (1961).
[5] M. Drescher *et al.*, Nature (London) **419**, 803 (2002).
[6] A. L. Cavalieri *et al.*, Nature (London) **449**, 1029 (2007).
[7] G. Sansone *et al.*, Nature (London) **465**, 763 (2010).
[8] M. Schultze *et al.*, Science **328**, 1658 (2010).
[9] V. S. Yakovlev *et al.*, Phys. Rev. Lett. **105**, 073001 (2010).
[10] H. G. Muller, Appl. Phys. B **74**, s17 (2002).
[11] P. M. Paul *et al.*, Science **292**, 1689 (2001).
[12] Y. Mairesse *et al.*, Science **302**, 1540 (2003).
[13] K. Varjú *et al.*, J. Mod. Opt. **52**, 379 (2005).
[14] S. Haessler *et al.*, Phys. Rev. A **80**, 011404 (2009).
[15] M. Swoboda *et al.*, Phys. Rev. Lett. **104**, 103003 (2010).
[16] V. Véniard, R. Taïeb, and A. Maquet, Phys. Rev. A **54**, 721 (1996).
[17] P. M. Dehmer *et al.*, J. Chem. Phys. **80**, 1030 (1984).
[18] M. Lein, Phys. Rev. Lett. **94**, 053004 (2005).
[19] A. Lofthus and P. H. Krupenie, J. Phys. Chem. Ref. Data **6**, 113 (1977).
[20] This approximation is here supported by the shape of the corresponding photoionization peak (at ~723 nm, see Fig. 3 of Ref. [17]), which presents a $q \sim 0$ Fano profile. Further investigations are required prior to extending it to any autoionizing state.
[21] We have removed the known harmonic phases from θ_{2q}, as done in the analysis of the experimental data in [14].
[22] Note that there is a frequency, close to 1.573 eV, for which the phases computed for $v' = 0$, 1, and 2 coincide simultaneously with the experimental ones.
[23] J. Caillat *et al.* (to be published).